



SEXUAL SELECTION

Adaptive introgression of a visual preference gene

Matteo Rossi^{1,2,*†}, Alexander E. Hausmann¹, Pepe Alcami¹, Markus Moest³, Rodaria Roussou¹, Steven M. Van Belleghem⁴, Daniel Shane Wright¹, Chi-Yun Kuo^{1,2,†}, Daniela Lozano-Urrego^{1,5}, Arif Maulana¹, Lina Melo-Florez^{1,5}, Geraldine Rueda-Muñoz^{1,5}, Saoirse McMahon¹, Mauricio Linares⁵, Christof Osman¹, W. Owen McMillan², Carolina Pardo-Diaz⁵, Camilo Salazar⁵, Richard M. Merrill^{1,2,*}

Visual preferences are important drivers of mate choice and sexual selection, but little is known of how they evolve at the genetic level. In this study, we took advantage of the diversity of bright warning patterns displayed by *Heliconius* butterflies, which are also used during mate choice. Combining behavioral, population genomic, and expression analyses, we show that two *Heliconius* species have evolved the same preferences for red patterns by exchanging genetic material through hybridization. Neural expression of *regucalcin1* correlates with visual preference across populations, and disruption of *regucalcin1* with CRISPR-Cas9 impairs courtship toward conspecific females, providing a direct link between gene and behavior. Our results support a role for hybridization during behavioral evolution and show how visually guided behaviors contributing to adaptation and speciation are encoded within the genome.

Organisms often use color and other visual cues to attract and recognize suitable mates (1). The evolution of these cues is increasingly understood at the molecular level, providing insights into the nature and origin of genetic variation on which selection acts, [e.g., (2–7)]. However, we know little of the genetic mechanisms underlying variation in the corresponding preferences, or of visually guided behaviors more broadly. Indeed, while progress has been made for other sensory modalities, and especially chemosensation [e.g., (8–10)], genetic studies of visual preference evolution remain limited to the identification of relatively broad genomic regions containing tens or hundreds of genes and/or are unable to distinguish between causal and correlated genetic changes (11–15). Although these studies have undoubtedly contributed to our understanding of population divergence, identifying the causal genes involved is key to uncovering how behavioral variation is generated during development and across evolutionary time.

Heliconius butterflies are well known for their diversity of bright warning patterns, which are also used as mating cues (16), perhaps alongside olfactory cues (17). Closely related taxa often display divergent wing patterns, and because males almost invariably prefer to court females that share their own color pattern, this contributes an important pre-

maturing reproductive barrier between species [e.g., (18)]. Although the genetics and evolutionary history of *Heliconius* color-pattern variation is well understood (19–25), we know little of the specific genetic mechanisms contributing to the evolution of the corresponding visual preference behaviors. Previously, we identified three genomic regions controlling differences in male courtship behaviors between the closely related sympatric species *H. cydno* and *H. melpomene*, which differ in color pattern (11). However, further fine mapping of this behavioral phenotype is impractical, and even the best supported of these behavioral quantitative trait loci (QTLs), which has also been explicitly linked to differences in visual preference (26), is associated with a confidence region containing 200 genes. Although patterns of neural gene expression highlight a number of candidates (27), the exact genes involved remain unknown.

Here we took advantage of the mimicry relationships among three closely related *Heliconius* species to determine how genetic variation for visual preferences has evolved in relation to that of the corresponding color-pattern cues. Whereas west of the Eastern Cordillera in the Andes, coexisting *H. cydno* and *H. melpomene* differ in forewing color (being white and red, respectively), on the eastern slopes, *H. cydno* is replaced by its sister species *H. timareta*, which shares the red patterns of the local *H. melpomene* (Fig. 1A). Mimicry between these two red species is not the result of independent mutations but of adaptive introgression, whereby *H. timareta* acquired color-pattern alleles following hybridization with *H. melpomene* (24, 25, 28). This presents an excellent opportunity to both (i) test whether behavioral phenotypes can similarly evolve through the reassembly of existing genetic variants on a novel genomic background and (ii) isolate the causal genes. We identified a region of increased admixture between

H. melpomene and *H. timareta* that is strongly associated with parallel preferences for red females in both species. We then leveraged this finding alongside transcriptomic analysis and genome editing to identify a major-effect gene underlying the evolution of visual preferences.

Evolution of parallel visual preference behaviors

To explore the evolution of visually guided behaviors across the *melpomene-cydno* group, we assayed mate preference for populations sampled across Colombia. Specifically, we tested *H. melpomene* and *H. timareta* males from the eastern slopes of the Eastern Cordillera, which both have a red forewing band, as well as *H. cydno* males from the western slopes of the Eastern Cordillera, which have a white or yellow forewing band. Male butterflies were simultaneously presented with a red *H. timareta* and a white *H. cydno* female in standardized trials. Males of the two red species showed a stronger preference for red females than the *H. cydno* males [differences in proportion of courtship time toward red females: *H. timareta* – *H. cydno* = 0.737 (0.630 to 0.844), *H. melpomene* – *H. cydno* = 0.713 (0.593 to 0.832); $n = 87$, $2\Delta\ln L = 99.8$, $P < 0.0001$] (Fig. 1B), but there was no difference in mate preference between the two red species [0.025 (–0.039 to 0.087)]. We confirmed that preference differences between male *H. timareta* and *H. cydno* are largely based on visual cues by repeating our experiment, this time presenting males with two *H. cydno* females, where the forewings of one female were artificially colored to match the red forewing of *H. timareta* (with respect to *Heliconius* color vision), and the wings of the other were “colored” with a transparent marker as a control [*H. timareta* – *H. cydno* = 0.46 (0.36 to 0.56); $n = 94$, $2\Delta\ln L = 53.7$, $P < 0.0001$] (fig S1). Overall, these results closely mirror previous data for Panamanian populations of *H. cydno* and *H. melpomene* (11, 18), in which the latter shows a much stronger preference for red females and confirms that although *H. timareta* is more closely related to *H. cydno*, it shares the visual preference phenotype of *H. melpomene*.

The same major-effect locus contributes to red preference in *H. melpomene* and *H. timareta*

If introgression has contributed to these parallel behavioral preferences for females with red patterns, we would expect the same genomic locations to influence the preference behaviors of both *H. melpomene* and *H. timareta*. In other words, we expect that the alleles at the location of the *H. melpomene* × *H. cydno* QTL to also segregate with preference differences in crosses between *H. timareta* and *H. cydno*. Confirming this, we found that genotype at the end of chromosome 18 is a strong

¹Faculty of Biology, LMU, Munich, Germany. ²Smithsonian Tropical Research Institute, Gamboa, Panama. ³Department of Ecology and Research Department for Limnology, Mondsee, University of Innsbruck, Innsbruck, Austria.

⁴Biology Department, University of Leuven, Leuven, Belgium.

⁵Faculty of Natural Sciences, Universidad del Rosario, Bogotá, Colombia.

*Corresponding author. Email: mrossi@rockefeller.edu (M.R.); merrill@bio.lmu.de (R.M.M.)

†Present address: Laboratory of Social Evolution and Behavior, The Rockefeller University, New York, USA.

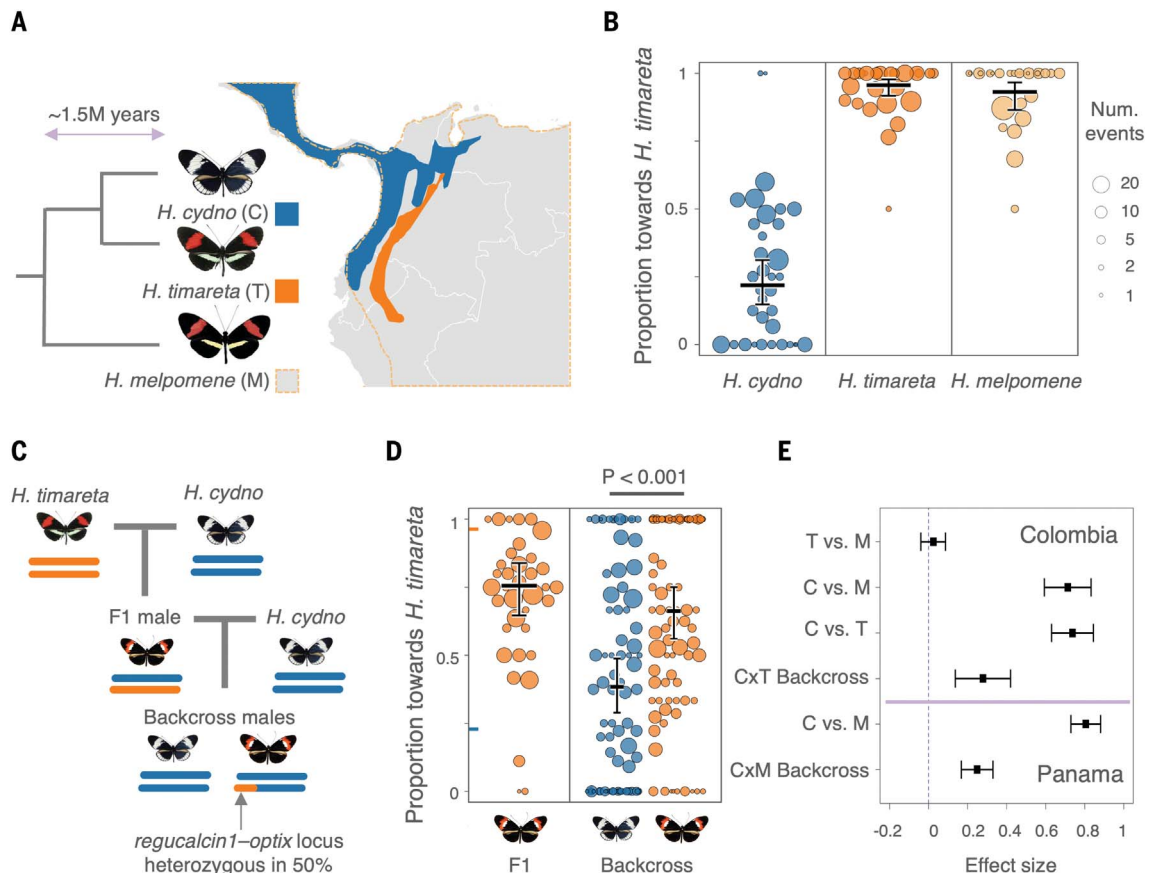
‡Present address: Department of Biological Science and Environmental Biology, Kaohsiung Medical University, Kaohsiung City, Taiwan.

Fig. 1. Parallel visual preferences are controlled by the same genomic region in the *Heliconius melpomene-cydn* group.

(A) *H. melpomene* (dotted orange line) co-occurs with *H. cydn* (blue) in Central America and South America to the west of the Eastern Cordillera in the Andes, whereas *H. melpomene* co-occurs with *H. timareta* (orange) to the east of the Eastern Cordillera.

H. melpomene and *H. timareta* share red warning patterns even though the latter is more closely related to the white/yellow *H. cydn*. (B) Proportion of courtship time directed toward red *H. timareta* females relative to white *H. cydn* females by males of the three species. Point size is scaled to the number of total minutes a male responded to either female type (a custom swarmplot was used to distribute dots

horizontally). Estimated marginal means and their 95% confidence intervals are displayed with black bars. (C) Crossing design for producing backcross hybrid individuals to *H. cydn* segregating at the behavioral QTL region on chromosome 18. (D) Relative courtship time directed toward red *H. timareta* females by F1 hybrid and backcross to *H. cydn* hybrid males. Orange points represent individuals that are heterozygous (i.e., “*cydn-timareta*”), and blue points represent individuals that are homozygous for *H. cydn* alleles at the QTL



predictor of male preference in *H. timareta* × *H. cydn* hybrids. Specifically, backcross hybrid males that inherit an allele from *H. timareta* at the previously detected QTL peak spent more time courting red *H. timareta* than courting white *H. cydn* females, as compared with their brothers that inherited two copies of the *H. cydn* alleles at the same location [differences in proportion of courtship time between males with “*cydn-timareta*” and “*cydn-cydn*” genotypes = 0.279 (0.137 to 0.42); $n = 157$, $2\Delta\ln L = 14.02$, $P = 0.00018$] (Fig. 1, C and D). The effect size observed here is almost identical to that seen in hybrids between *H. cydn* and *H. melpomene* [i.e., 0.249 (0.168 to 0.33)] (Fig. 1E).

To further confirm that the QTL region on chromosome 18 specifically modulates visual mate preferences, we also assayed mate preference behaviors of *H. timareta* × *H. cydn* hybrid males toward white (transparently painted) and red-painted *H. cydn* females (as described

above). We found that backcross males heterozygous for *H. timareta* and *H. cydn* alleles at the QTL confidence region on chromosome 18 court red-painted females more frequently than do their brothers homozygous for the *H. cydn* allele ($n = 270$, $2\Delta\ln L = 7.811$, $P = 0.005$) (fig. S1). Although the effect size for this experiment [0.0778 (0.024 to 0.13)] is reduced compared with that seen for experiments that use *H. timareta* females, this still represents a considerable proportion of the observed parental difference (~17%). Together, our two experiments confirm that the same genomic region at the end of chromosome 18 modulates variation in visual mate preferences across the *melpomene-cydn* group.

Genomic signatures of adaptive introgression at the preference locus

To further determine whether introgression of preference alleles has contributed to behavioral evolution in these species, we next

peak/*optix* region on chromosome 18. Although we observe evidence of recombination in our crosses, the QTL peak/*optix* region on chromosome 18 often segregates with warning pattern (see supplementary materials, materials and methods). (E) Differences in estimated marginal means for relative courtship time between butterfly types tested in Colombia (this study) and in Panama (11). T = *H. timareta*, M = *H. melpomene*, C = *H. cydn*, Backcross = backcross to *H. cydn* hybrids.

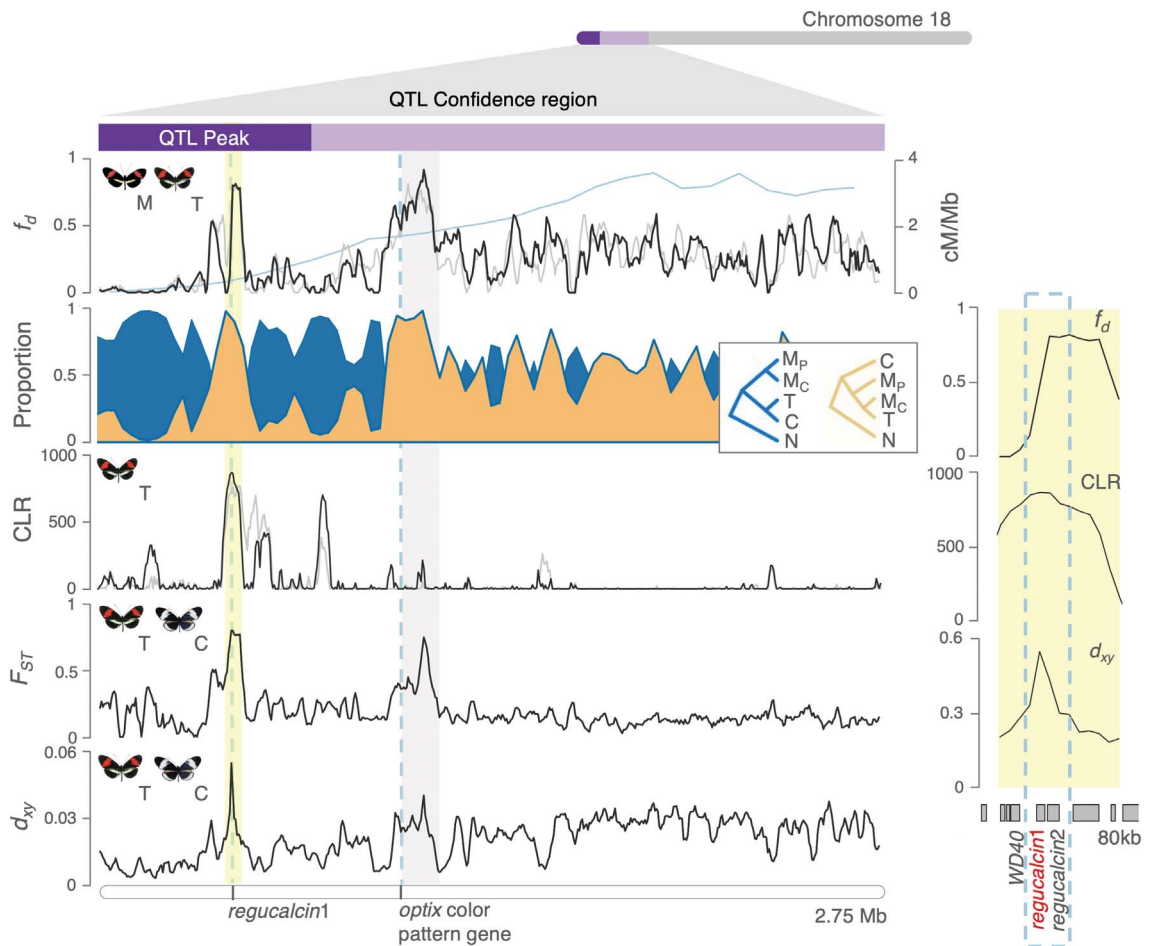
analyzed admixture proportions [f_d , (29)] between sympatric red-preferring *H. melpomene* and *H. timareta*. We observed two notable peaks of admixture in the QTL region on chromosome 18, located within the behavioral QTL peak (i.e., the region of greatest statistical association with difference in male preference between *H. cydn* and *H. melpomene*) and upstream of the adjacent major color-pattern gene, *optix*, corresponding to its putative regulatory region (5, 30) (Fig. 2; see also fig. S2). Admixture estimates are repeatable across geographic populations of *H. melpomene* and *H. timareta* and are independent of variation in local recombination rates, which are known to otherwise correlate with admixture proportions (31) (Fig. 2).

Introgression at the two loci on chromosome 18 is further supported by analyses with *Twisst* (32), which quantifies the proportion of different phylogenetic relationships among individuals of different species across the

Fig. 2. Different genomic signatures support both divergence and adaptive introgression at the *regucalcin* locus. (Left, top row) Admixture proportion values (20-kb windows) between *H. melpomene* and *H. timareta* at the behavioral QTL region on chromosome 18 (*x* axis indicates physical position) for Colombian (black) and Peruvian (gray) populations, with recombination rate overlaid in blue. (Left, second row) Topology weightings (proportions of a particular phylogenetic tree over all possible rooted trees) are shown for the species (blue) and introgression (orange) trees [50-SNP (single-nucleotide polymorphism) windows; a LOESS (locally estimated scatterplot smoothing) function across 150-kb windows was applied]. *H. numata* was used as the outgroup. (Left, third row) Composite likelihood ratio (CLR) of a selective sweep in *H. timareta* (50-SNP windows). (Left, fourth

and fifth rows) Fixation index (F_{ST}) and d_{xy} , measures of genetic differentiation and divergence between *H. timareta* and *H. cydno*. Extending from top to bottom, vertical light-blue dotted lines highlight the gene coordinates of the candidate gene for behavioral difference *regucalcin1*, as well as the color-pattern gene *optix* (~550 kb apart), and gray shading indicates putative

regulatory regions of *optix* affecting color pattern. The QTL confidence region contains 200 genes (46). (Right) Panel zooms into the region containing candidate behavioral genes. M, T, C, and N denote *H. melpomene*, *H. timareta*, *H. cydno*, and *H. numata*, respectively; subscripts _P and _C denote Panama and Colombia, respectively.



chromosome. In these analyses, the introgression topology, in which *H. timareta* and *H. melpomene* cluster together with *H. cydno* as an outgroup, is strongly supported both within the QTL peak and at *optix* (Fig. 2 and fig. S3). These admixture peaks of approximately 30 and 150 kb, respectively, additionally coincide with elevated levels of genetic differentiation (F_{ST}) and absolute genetic divergence (d_{xy}) between red- and white-preferring populations (Fig. 2). Patterns of linkage disequilibrium between these two loci are consistent with the genetic associations predicted to arise between cue and preference alleles as a result of assortative mating (8, 33) (fig. S4). Lastly, using *Sweepfinder2* (34), we found evidence for a recent selective sweep in *H. timareta* (top 1% quantile across autosomes), which is coincident with the peak of increased admixture within the behavioral QTL peak described above, but not at *optix* (Fig. 2 and fig. S5). These results suggest adaptive introgression of alleles from

red-preferring *H. melpomene* into *H. timareta* at a genomic location strongly associated with variation in visual preference.

Cis-regulated expression differences of *regucalcin1* are associated with visual preference

We next generated RNA sequencing (RNAseq) libraries for combined eye and brain tissue from adult males across all populations tested in our preference assays to determine whether consistent differences in gene expression are associated with the behavioral QTL on chromosome 18. We sampled at the adult stage, reasoning that if the neural mechanism underlying divergent preference behaviors involves a change in neuronal activity, this might require sustained transcription. Of 200 genes within the chromosome 18 QTL candidate region—although a number were differentially expressed in individual comparisons (fig. S6)—only one was consistently differentially expressed across

all red- and white-preferring population comparisons (reared under common garden conditions, fig. S7). Specifically, *regucalcin1*, which perfectly coincides with the peak of adaptive introgression between red-preferring populations detected as described above, shows lower expression in the neural tissue of Panamanian and Colombian populations of *H. melpomene* and *H. timareta*, all of which we have shown to have a red preference as compared with *H. cydno* (Fig. 3A and fig. S7). Expression of *regucalcin1* is also significantly reduced in *H. melpomene amaryllis* and *H. melpomene melpomene* as compared with *H. cydno*, two populations also known to display a preference for red females (18, 35) (fig. S7). Immunostainings in adult male *H. melpomene* revealed expression patterns of *regucalcin1* in the visual pathways across the brain, predominantly in somata, especially the nuclei, and also in neuropil, as well as in the eye (Fig. 3C and fig. S8). Although this does not pinpoint the

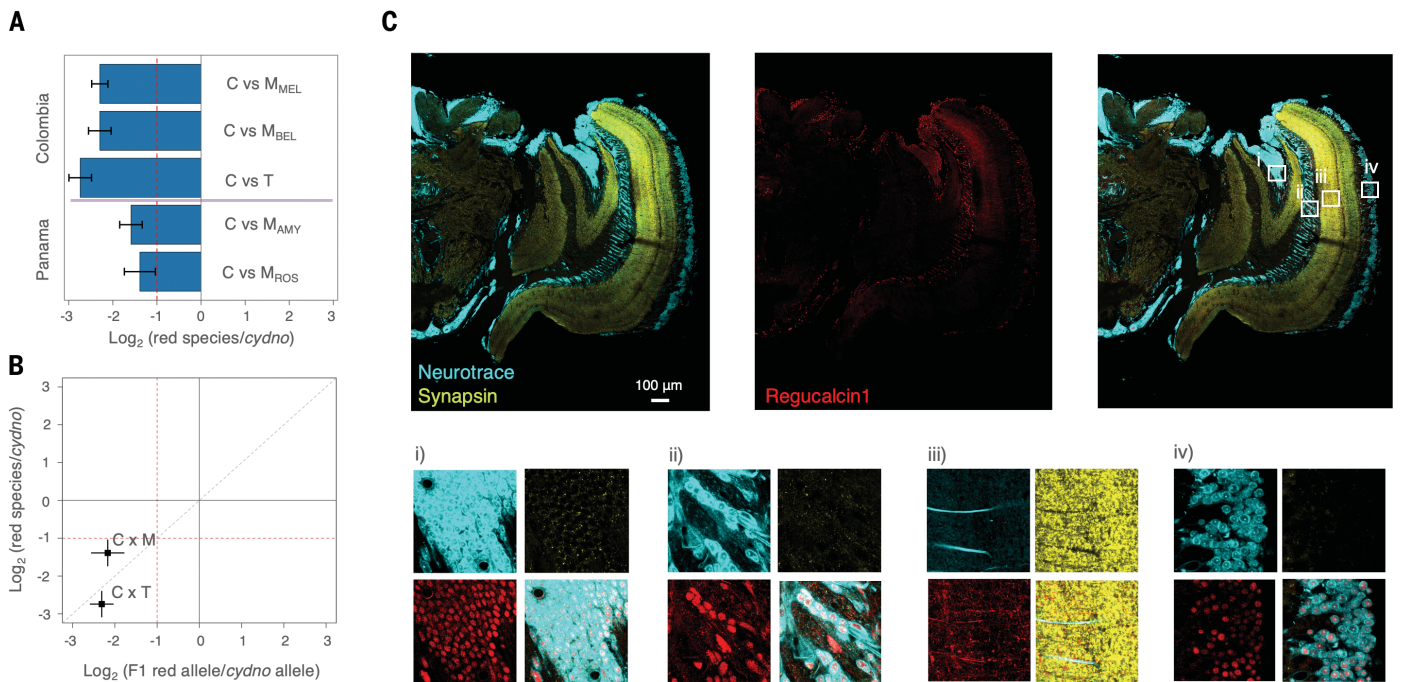


Fig. 3. Cis-regulated expression differences of *regucalcin1* are associated with visual preference, and *regucalcin1* is expressed in the visual pathways. (A) *Regucalcin1* is differentially expressed between red- and white-preferring butterflies. Bar widths represent the value and black lines the standard error of the (base 2) logarithmic fold change in expression between red- and white-preferring *Heliconius* subspecies (comparisons conducted only between butterflies raised in the same insectary locations). The dashed red line indicates the threshold for a twofold change in mRNA expression. M, T, and C denote *H. melpomene*, *H. timareta*, and *H. cydn0*, respectively; subscripts MEL, BEL, AMY, and ROS denote subspecies names *melpomene*, *bellulla*, *amaryllis*, and *rosina*, respectively. (B) Allele-specific expression analyses indicate that differences in expression of *regucalcin1* in the brains of red- and white-preferring

population are *cis*-regulated. Points indicate the value and bars the standard error of the log₂ (fold change) in expression between parental species (vertical) and the alleles in F1 hybrids (horizontal), for *regucalcin1*. Dashed red lines indicate the threshold for a twofold change in expression for the genes in the species (horizontal), and for the alleles in the hybrids (vertical). *Regucalcin1* is largely *cis*-regulated (indicated by proximity to $y = x$). (C) *Regucalcin1* is widely expressed in *H. melpomene* brains, including the visual pathways and eyes (fig. S8). (Top) Immunostaining of the brain hemisphere, from left to right: (left) counterstaining of somata with NeuroTrace and of the neuropil with synapsin; (center) staining against *regucalcin1*; (right) merged image. (Bottom) Enlargement of somata (i), (ii), and (iv), where the signal is particularly strong in nuclei, and neuropil (iii) along the visual pathways.

particular mechanism of action, it confirms that regulatory changes of *regucalcin1* can affect visual preference behavior.

If expression differences in *regucalcin1* are responsible for the behavioral variation associated with the QTL on chromosome 18, they must result from changes within the *cis*-regulatory regions of the genes themselves, as opposed to those of other *trans*-acting genes elsewhere in the genome. To test whether differences in gene-expression levels between parental species were due to *cis*- or *trans*-regulatory changes, we conducted allele-specific expression analyses in adult male F1 *H. melpomene* × *H. cydn0* and *H. cydn0* × *H. timareta* hybrids. In F1 hybrids, both parental alleles are exposed to the same *trans* environment, and consequently *trans*-acting factors will act on alleles derived from each species equally (unless there is a change in the *cis*-regulatory regions of the respective alleles). Confirming *cis* regulation of *regucalcin1*, we found a significant twofold up-regulation of the *H. cydn0* allele relative to the *H. melpomene* or

H. timareta allele in the neural tissue of both our *H. melpomene* × *H. cydn0* and *H. timareta* × *H. cydn0* F1 males (Wald test all comparisons: $P < 0.001$, Fig. 3B).

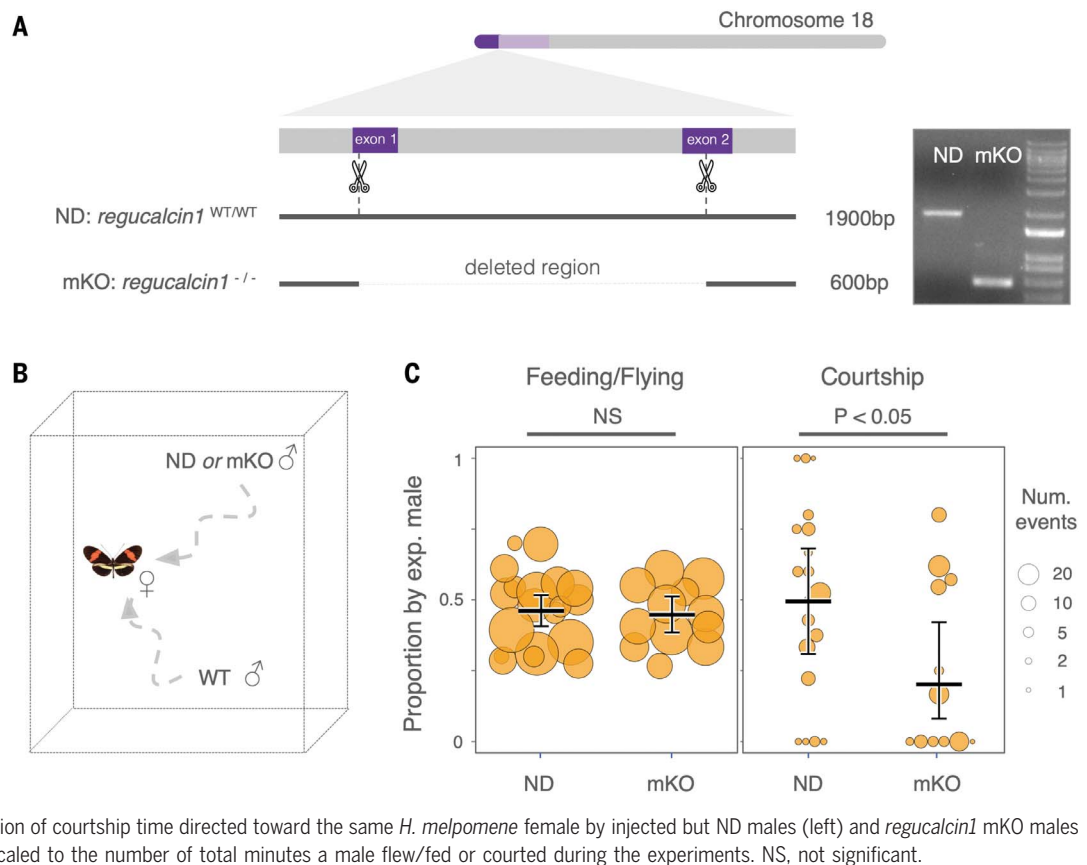
CRISPR-Cas9 mediated knockout of *regucalcin1* disrupts male courtship behaviors

Combining genetic crosses and behavioral data, as well as population genomic and expression analyses, our results strongly implicate *regucalcin1* as a visual preference gene. To functionally test for a link between gene and behavior, we deleted part of the protein-coding region of *regucalcin1* in *H. melpomene* individuals by introducing a ~1300-base pair (bp) deletion spanning most of its first and second exon using CRISPR-Cas9 (Fig. 4A). In trials with a single conspecific female (Fig. 4B), mosaic knockout (mKO) males (i.e., those with a deletion at *regucalcin1* in a substantial number of cells, including in brain tissue, fig. S9) were significantly less likely to court than control (ND) males without the deletion [difference in proportion of minutes courting, trials

with mKO males – trials with ND males = 0.24 (0.03 to 0.55); $2\Delta\ln L = 4.51$, $P < 0.05$] (Fig. 4C). mKO individuals may suffer decreased viability both before and after eclosion (fig. S10), and some mKO butterflies were unable to fly (8/44 individuals), as determined in our “drop test” [as compared with 0/40 ND individuals or 0/42 wild-type (WT) individuals; Fisher exact test: $P < 0.001$]. However, only surviving males that could fly were included in our courtship trials. Furthermore, all mKO (36/36), ND (31/31), and WT (30/30) individuals tested, including seven individuals that failed the subsequent “drop test,” showed an optomotor response (movie S1), suggesting that basic visual sensorimotor skills are largely intact in mKO individuals. Lastly, we observed no difference in the proportion of time flying or feeding between the same mKO or ND males included in our courtship trials [0.01 (–0.07 to 0.097); $2\Delta\ln L = 0$, $P > 0.9$] (Fig. 4C and fig. S11). In other words, courtship, but not other behaviors, was significantly reduced in *regucalcin1* KO males as compared with controls, which

Fig. 4. Disruption of *regucalcin1* with CRISPR-Cas9 impairs male courtship behavior.

(A) (Left) Schematic representation of the *regucalcin1* locus with the target sites of the small guide RNAs and resulting CRISPR-Cas9-mediated deletion of ~1300 bp. (Right) Gel electrophoresis of polymerase chain reaction (PCR)-amplified *regucalcin1* fragments from individuals without (ND, nondeletion) and with deletion (mKO, mosaic knockout) at *regucalcin1*.



(B) Schematic representation of courtship trials. Experimental (i.e., mKO or ND) males that passed our “drop test” were paired with a WT male and introduced into a cage with a WT virgin *H. melpomene* female. This paired design allowed us to control for the injection procedure, as well as for prevailing conditions that might potentially influence male behavior.

(C) (Left) Proportion of time spent flying or feeding by experimental (“exp”) males—those injected but ND males or *regucalcin1* mKO males—relative to WT males. (Right) Proportion of courtship time directed toward the same *H. melpomene* female by injected but ND males (left) and *regucalcin1* mKO males relative to WT males. Point size is scaled to the number of total minutes a male flew/fed or courted during the experiments. NS, not significant.

retain functional copies of *regucalcin1*. This finding provides functional evidence that *regucalcin1* has a specific effect on male courtship behavior and that this effect is not due to a more general impairment of behavior.

Conclusions

Hybridization has been suggested to be an important source of genetic variation on which selection can act, including during behavioral evolution (36, 37), but direct links between specific causal genes and behavioral phenotypes are lacking. Our results strongly suggest that *H. timareta* acquired a *regucalcin1* allele by hybridizing with its closely related comimic *H. melpomene*, increasing attraction toward red females and presumably reproductive success. By contrast, where *H. melpomene* co-occurs with the equally closely related but differently colored *H. cydno*, *regucalcin1* contributes an important barrier to interspecific gene flow through its contribution to divergent mating preferences (11, 38). As such, the evolutionary impact of *regucalcin1* depends on the local mimetic landscape, emphasizing the complex role that hybridization may have on population divergence by reassembling genetic variants (39).

Although other genes aside from *regucalcin1* undoubtedly contribute to visual preference evolution in *Heliconius*, there is little evidence

that these include major wing-patterning genes. There is no evidence for differential expression of *optix* between red- and white-preferring populations, and protein-coding differences similarly do not exist (27). Instead, our data suggest that although variation in red-color cue and preference map to the same genomic region, they are encoded by separate loci regulating the expression of *optix* (19) and *regucalcin1*, respectively (fig. S12). By ensuring robust genetic associations between components of reproductive isolation, physical linkage is expected to facilitate speciation with gene flow (40), and this is likely the case for the differently colored species *H. cydno* and *H. melpomene* (11). However, our present results suggest that these loci can also evolve independently, and evidence of a recent selective sweep in *H. timareta* at *regucalcin1*, but not *optix*, as well as distinct peaks of admixture between red-preferring species at these two genes, suggest separate introgression events. It seems likely that the acquisition of red patterns in *H. timareta* was immediately advantageous given strong selection for mimicry of local warning patterns, whereas the corresponding male preference would become advantageous only when conspecific red females had already increased in frequency.

Other prominent examples of visual preference evolution have emphasized the role of selec-

tion imposed by the broader sensory environment. In cichlid fish, for example, divergent mating preferences may have evolved as a by-product of environmental selection acting on visual-pigment genes (15, 41). By contrast, *H. timareta* and *H. melpomene* have evolved parallel visual preferences despite inhabiting divergent light environments (*H. timareta* is found in forest habitats similar to those of *H. cydno*), to which the neural and sensory systems are otherwise adapted (42). This suggests that visual preference evolution in *Heliconius* is not the by-product of divergent selection imposed by the broader sensory environment but rather a consequence of direct selection to find receptive females, perhaps strengthened through reinforcement (by which selection favors increased premating barriers to avoid the production of less-fit hybrids) (18, 43, 44).

Overall, our study indicates that the evolution of *cis*-regulated differences in *regucalcin1* expression contributes to divergent mating preferences in *Heliconius* and that hybridization can be an important source of genetic variation during behavioral evolution. The function of *regucalcin* has not been well characterized, although it seems to be involved in calcium homeostasis and signaling (45). Our CRISPR-mediated *regucalcin1* deletion impaired survival and flight in a few mosaic butterflies, supporting a broad role across biological

processes. However, in other mosaic KO individuals, we observed a significant reduction in mate attraction behaviors, independent of more general impairment of motor activity, implying specific effects on male mating behavior. *Regucalcin1* expression differences, sustained in adult brain and/or eye tissue, likely alter how visual information is processed or integrated to determine divergent mating preferences. The challenge now is to determine the molecular and neural mechanisms through which *regucalcin1* acts.

REFERENCES AND NOTES

1. I. C. Cuthill *et al.*, *Science* **357**, eaan0221 (2017).
2. A. Orteu, C. D. Jiggins, *Nat. Rev. Genet.* **21**, 461–475 (2020).
3. U. Knief *et al.*, *Nat. Ecol. Evol.* **3**, 570–576 (2019).
4. S. Ansaï *et al.*, *Nat. Commun.* **12**, 1350 (2021).
5. S. M. Van Belleghem *et al.*, *Science* **379**, 1043–1049 (2023).
6. M. Liang *et al.*, *Science* **379**, 576–582 (2023).
7. V. Ficarrotta *et al.*, *Proc. Natl. Acad. Sci. U.S.A.* **119**, e2109255118 (2022).
8. M. Unbehend *et al.*, *Nat. Commun.* **12**, 2818 (2021).
9. P. Brand *et al.*, *Nat. Commun.* **11**, 244 (2020).
10. O. M. Ahmed *et al.*, *Cell Rep.* **27**, 2527–2536.e4 (2019).
11. R. M. Merrill *et al.*, *PLOS Biol.* **17**, e2005902–e2005921 (2019).
12. M. R. Kronforst *et al.*, *Proc. Natl. Acad. Sci. U.S.A.* **103**, 6575–6580 (2006).
13. S. R. Pryke, *Evolution* **64**, 1301–1310 (2010).
14. N. L. Chamberlain, R. I. Hill, D. D. Kapan, L. E. Gilbert, M. R. Kronforst, *Science* **326**, 847–850 (2009).
15. O. Seehausen *et al.*, *Nature* **455**, 620–626 (2008).
16. J. Crane, *Zoologica* **40**, 167–196 (1955).
17. K. Darragh *et al.*, *PeerJ* **5**, e3953 (2017).
18. C. D. Jiggins, R. E. Naisbit, R. L. Coe, J. Mallet, *Nature* **411**, 302–305 (2001).
19. R. D. Reed *et al.*, *Science* **333**, 1137–1141 (2011).
20. N. J. Nadeau *et al.*, *Nature* **534**, 106–110 (2016).
21. A. Martin *et al.*, *Proc. Natl. Acad. Sci. U.S.A.* **109**, 12632–12637 (2012).
22. E. L. Westerman *et al.*, *Curr. Biol.* **28**, 3469–3474.e4 (2018).
23. N. B. Edelman *et al.*, *Science* **366**, 594–599 (2019).
24. R. W. R. Wallbank *et al.*, *PLOS Biol.* **14**, e1002353 (2016).
25. Heliconius Genome Consortium, *Nature* **487**, 94–98 (2012).
26. R. M. Merrill, B. Van Schooten, J. A. Scott, C. D. Jiggins, *Proc. Biol. Sci.* **278**, 511–518 (2011).
27. M. Rossi *et al.*, *Nat. Commun.* **11**, 4763 (2020).
28. C. Pardo-Diaz *et al.*, *PLOS Genet.* **8**, e1002752 (2012).
29. S. H. Martin, J. W. Davey, C. D. Jiggins, *Mol. Biol. Evol.* **32**, 244–257 (2015).
30. J. J. Lewis *et al.*, *Proc. Natl. Acad. Sci. U.S.A.* **116**, 24174–24183 (2019).
31. S. H. Martin, J. W. Davey, C. Salazar, C. D. Jiggins, *PLOS Biol.* **17**, e2006288 (2019).
32. S. H. Martin, S. M. Van Belleghem, *Genetics* **206**, 429–438 (2017).
33. M. Kirkpatrick, *Evolution* **36**, 1–12 (1982).
34. M. DeGiorgio, C. D. Huber, M. J. Hubisz, I. Hellmann, R. Nielsen, *Bioinformatics* **32**, 1895–1897 (2016).
35. C. Mèrot, B. Frérot, E. Leppik, M. Joron, *Evolution* **69**, 2891–2904 (2015).
36. J. I. Meier *et al.*, *Nat. Commun.* **10**, 5391 (2019).
37. Q. Helleu, C. Roux, K. G. Ross, L. Keller, *Proc. Natl. Acad. Sci. U.S.A.* **119**, e2201040119 (2022).
38. D. R. Laetsch *et al.*, *PLOS Genet.* **19**, e1010999 (2023).
39. D. A. Marques, J. I. Meier, O. Seehausen, *Trends Ecol. Evol.* **34**, 531–544 (2019).
40. J. Felsenstein, *Evolution* **35**, 124–138 (1981).
41. M. E. Maan, O. Seehausen, T. G. G. Groothuis, *Am. Nat.* **189**, 78–85 (2017).
42. S. H. Montgomery, M. Rossi, W. O. McMillan, R. M. Merrill, *Proc. Natl. Acad. Sci. U.S.A.* **118**, e2015102118 (2021).
43. M. R. Kronforst, L. G. Young, L. E. Gilbert, *J. Evol. Biol.* **20**, 278–285 (2007).
44. R. M. Merrill *et al.*, *J. Evol. Biol.* **28**, 1417–1438 (2015).
45. M. Yamaguchi, *Integr. Biol. (Camb.)* **4**, 825–837 (2012).
46. M. Rossi *et al.*, *SpeciationBehaviour/Adaptive_introgession_of_a_visual_preference_gene*, version v1, Zenodo (2023); <https://doi.org/10.5281/zenodo.10203687>.

ACKNOWLEDGMENTS

We dedicate this paper to the memory of our friend and colleague A. E. Hausmann. We are grateful to B. Hoelldobler, I. Leon, F. Rossi, R. Stephens, S. Smith, J. Borrero, M. Freire, A. Comin, C. Burrows, M. Bauer, Y.-P. Toh, and C. Rottenberger for technical and rearing assistance; B. Grothe for providing research infrastructure; and M. Choteau for help with fieldwork. We thank F. Cicconardi for sharing a pipeline for ISO-Seq

analysis and S. Martin for sharing vcf files. We thank P. Brand, M. Farnworth, N. Gompel, J. Hanly, L. Livraghi, R. Pereira, J. Wolf, S. Montgomery, and V. Warmuth for valuable input on methods and the manuscript. We thank the Universidad del Rosario and the Smithsonian Tropical Research Institute for providing butterfly maintenance and rearing support in Colombia and Panama, respectively. We are grateful to Autoridad Nacional de Licencias Ambientales, Colombia (permit 530) and the Ministerio de Ambiente, Panama (permit SE/AP-14-18) for permission to collect butterflies. **Funding:** This research was supported by Deutsche Forschungsgemeinschaft (DFG) Emmy Noether grant GZ:ME 4845/1-1 (R.M.M.) and ERC starting grant 851040 (R.M.M.). **Author contributions:** Conceptualization: R.M.M. Methodology: M.R., A.E.H., P.A., D.S.W., and R.M.M. Investigation: M.R., A.E.H., P.A., R.R., D.L.-U., C.-Y.K., L.M.-F., G.R., S.M., and R.M.M. Formal analysis: M.R., A.E.H., P.A., S.M.V.B., M.M., A.M., and R.M.M. Visualization: M.R., A.E.H., P.A., and R.M.M. Funding acquisition: R.M.M. Project administration: M.L., W.O.M., C.P.-D., C.S., and R.M.M. Supervision: P.A., W.O.M., C.O., C.P.-D., C.S., and R.M.M. Writing – original draft: M.R. and R.M.M. Writing – review and editing: All authors. **Competing interests:** The authors declare that they have no competing interests. **Data and materials availability:** Custom scripts, analyses pipelines, and raw data are available through the archived Zenodo repository (46). Whole-genome resequencing, RNA-Seq, and ISO-Seq data are available at the European Nucleotide Archive (ENA): <https://www.ebi.ac.uk/ena/browser/view/PRJEB69696>. Previously compiled data were retrieved from ENA with the following accession numbers: PRJEB39935, PRJEB35570, and PRJEB1749. More information can be found in data S1. **License information:** Copyright © 2024 the authors, some rights reserved; exclusive licensee American Association for the Advancement of Science. No claim to original US government works. <https://www.science.org/about/science-licenses-journal-article-reuse>

SUPPLEMENTARY MATERIALS

science.org/doi/10.1126/science.adj9201

Materials and Methods

Figs. S1 to S12

Tables S1 and S2

References (47–89)

Movie S1

Data S1

MDAR Reproducibility Checklist

Submitted 24 July 2023; accepted 30 January 2024

[10.1126/science.adj9201](https://doi.org/10.1126/science.adj9201)